Chromosome-level assemblies of multiple *Arabidopsis thaliana* accessions reveal hotspots of genomic rearrangements

Wen-Biao Jiao and Korbinian Schneeberger*

Max Planck Institute for Plant Breeding Research, Department for Plant Developmental Biology, Carl-von-Linné-Weg 10, 50829 Cologne, Germany

* Author for correspondence: schneeberger@mpipz.mpg.de

We report chromosome-level, reference-quality assemblies of seven *Arabidopsis thaliana* accessions selected across the geographic range of this model plant. Each genome assembly revealed between 13-17 Mb of rearranged and 5-6 Mb of novel sequence introducing copy-number changes in ~5000 genes, including ~1,900 genes which are not part of the current reference annotation. By analyzing the collinearity between the genomes, we identified ~350 hotspots of rearrangements covering ~4% of the euchromatic genome. Hotspots of rearrangements are characterized by accession-specific accumulation of tandem duplications and are enriched for genes implicated in disease resistance and secondary metabolite biosynthesis. Loss of meiotic recombination in hybrids within these regions is consistent with the accumulation of rare and deleterious alleles and incompatibility loci. Together this suggests that hotspots of rearrangements are governed by different evolutionary dynamics as compared to the rest of the genome and facilitate rapid responses to the ever-evolving challenges of biotic stress.

The first complete assembly of a plant genome, the reference sequence of *A. thaliana* (Col-0), was based on a minimal tiling path of BACs sequenced with Sanger technology and was released in the year 2000[1]. Since then, this reference has been widely used for identification of genetic variants, which typically relied on short-read based resequencing or reference-guided assembly[2–8]. Although millions of small variants have been identified, the identification of large genomic rearrangements remained challenging. In contrast, reference-independent, chromosome-level assemblies promise accurate identification of all sequence differences independent of their complexity[9]. So-far, however, there are only few reports on

35 whole-genome *de-novo* assemblies for *A. thaliana* available and the assemblies have not
36 been thoroughly compared to each other[10–13].
37 Using deep PacBio (45-71x) and Illumina (56-78x) whole-genome shotgun sequencing,
38 we assembled the genomes of seven accessions from geographically diverse populations
39 including An-1 (Antwerpen, Belgium), C24 (Coimbra, Portugal), Cvi-0 (Cape Verde Islands),
40 Eri-1 (Eringsboda, Sweden), Kyo (Kyoto, Japan), L*er* (Gorzów Wielkopolski, Poland) and Sha
41 (Shahdara, Tadjikistan) (Supplementary Table 1). The assembly of L*er* was already described
42 in a recent study and used for the development of a whole-genome comparison tool[9], however,
43 as it was generated in the same process it is integrated in this study as well. These accessions
44 (together with the reference accession Col-0) were initially selected as the founder lines of
45 Arabidopsis Multi-parent Recombination Inbreeding Lines (AMPRIL)[14] population. The contig
46 assemblies featured N50 values from 4.8 - 11.2 Mb and chromosome-normalized L50
47 (CL50)[15] values of 1 or 2 indicating that nearly all chromosome arms were assembled into a
48 few (typically one to five) contigs only (Table 1 and Supplementary Table 2). We generated
49 chromosome-level assemblies based on the homology of these contigs to the reference
50 sequence and validated the resultant contig order of two of the assemblies with three different
51 genetic maps, where we did not find evidence for a single mis-placed contig (Supplementary
52 Table 3). The seven chromosome-level assemblies consisted of 43 - 73 contigs and reached
53 a total length of 117.7 - 118.8 Mb, which is very similar to the 119.1 Mb of the reference
54 sequence (Fig. 1 and Table 1) and even included parts of the highly complex regions of
55 centromeres, telomeres and rDNA clusters (Supplementary Table 4 and 5). The remaining
56 unanchored contigs had a total length of 1.5 - 3.3 Mb and consisted almost entirely of repeats,
57 which agrees with gaps between the contigs, which most of them (84.5% - 98.0%) were
58 introduced due to repetitive regions (Supplementary Table 6).
59 Between 99.1% and 99.4% of the reference genes[16] could be aligned to each of the
60 seven assemblies. Almost all of the remaining genes were truly missing in the genomes as
61 we could confirm by mapping their Illumina short reads against the reference sequence
62 (Supplementary Table 7), suggesting that the assemblies covered almost all of the genic
63 regions. In agreement with this, we annotated 27,098 to 27,574 protein-coding genes in each
64 of the assemblies, which is similar to the 27,445 genes annotated in the reference sequence[16]
65 (Table1, Supplementary Table 8 and 9).
66 The lack of contiguity of short sequencing reads makes resequencing-based analyses
67 mostly blind for large rearrangements. In contrast, the high contiguity of these new assemblies
68 now enables the comprehensive description of complex structural rearrangements including
69 inversions, translocations and duplications (Fig. 2a). By comparing each of the new
70 assemblies against the reference sequence using the whole-genome comparison tool *SyRI*[9],
71 we found between 102.2 and 106.6 Mb of syntenic regions and between 12.6 and 17.0 Mb of

rearranged regions in each of the genomes. The rearrangements included 1.5 - 4.2 Mb (33 - 46) inversions, 1.0 - 1.7 Mb (364 - 566) intra-chromosome translocations, and 0.9 - 1.3 Mb (365 - 626) inter-chromosome translocations. Apart from balanced structural variation, we also found 7.2 – 8.7 Mb (4,288 – 5,150) of duplication loss and gain variation (Fig. 2b and Supplementary Table 10). Similar to sequence variation, rearrangements were not evenly distributed along the chromosomes, but were enriched in pericentromeres (Supplementary Table 11). Their lengths ranged from a few dozen bp to hundreds of kb and even Mb scale (Fig. 2c). Among the largest differences were inversions including a 2.48 Mb inversion on chromosome 3 of Sha (Supplementary Fig. 1 and Supplementary Table 12), which is consistent with the earlier observation of suppressed meiotic recombination in this region in hybrids including the Sha haplotype[17,18]. Local sequence differences in rearranged regions were generally more frequent as compared to syntenic regions mostly due to an excess of sequences with different copy-number variation (Fig. 2d, Supplementary Fig. 2 and Supplementary Table 13). Overall, the allele frequencies of balanced rearrangements like inversions and translocations were generally lower as compared to duplications, where more than 50% of them were shared by at least two accessions suggesting differences in the selection pressures acting on balanced and non-balanced variation (Fig. 2e).

In each of the pairwise comparisons, we identified 5.1 - 6.5 Mb accession-specific sequence (Fig. 2b). Using these regions and their overlaps for a pan-genome analysis[19,20], we estimated a pan-genome size of ~135 Mb and a core-genome size of ~105 Mb (Fig. 2f). A similar analysis with genes modelled a gene pan-genome size of ~30,000 genes illustrating that one reference genome is not sufficient to capture the entire sequence diversity within *A. thaliana* (Supplementary Fig. 3).

Genomic rearrangements have the potential to delete, create or duplicate genes resulting in gene copy number variation (CNV). Based on gene family clustering of all genes in all eight accessions[21] we found 22,040 gene families with conserved copy number, while 4,957 gene families showed differences in gene copy numbers (Fig. 2g and Supplementary Table 14). Almost 99% of the copy-variable gene families had 5 or less copies, while only less than 10% of them showed more than two different copy numbers across the eight accessions (Supplementary Fig. 4). Among the copy-variable genes we found 1,941 non-reference gene families including 891 gene families present in at least two of the other accessions (Fig. 2h). Around 23% of the non-reference gene families featured orthologs in the closely related genome of *Arabidopsis lyrata* and, according to RNA-seq read mapping, 26%-40% of them showed evidence of expression in the individual accessions (Supplementary Table 15). The remaining 1,050 non-reference gene families, which were evenly distributed across the accessions (Fig. 2g), with the only exception of Cvi-0, where we found nearly twice as many (214) accession-specific genes which is in agreement with the divergent ancestry of this relict

109 accession[4,22].

110 The high contiguity of the assembled sequences enabled the first analysis of the
111 conservation of collinearity between different Arabidopsis genomes. For this we introduced a
112 new concept called *Synteny Diversity* π_{syn}, which is similar to *Nucleotide Diversity*[23], however,
113 instead of measuring average sequence differences it measures average fraction of non-
114 collinear genome pairs in a given population. π_{syn} values can range from 0 to 1, where 1 refers
115 to the complete absence of collinearity between any of the genomes and 0 to regions where
116 all genomes are collinear. π_{syn} can be calculated in any given region, however, the annotation
117 of synteny still needs to established within the context of the whole genomes to avoid false
118 assignments of homologous but non-allelic sequence (Methods).

119 We calculated π_{syn} in 5-kb sliding windows across the genome using pair-wise
120 comparisons of all eight accessions (Fig. 3a). As expected, π_{syn} was generally high in
121 pericentromeric regions and low in chromosome arms. Overall, this revealed around 90 Mb
122 (76% of the genome) where all genomes were syntenic to each other, while for the remaining
123 29 Mb (24%) the collinearity between the genomes was not conserved. This, for example,
124 included a region on chromosome 3 (ranging from Mb ~2.8 - 5.3), where π_{syn} was increased
125 to ~0.25 due to the 2.48 Mb inversion specific to Sha (Fig. 3a, arrow labelled with (a)).

126 Unexpectedly, however, some regions featured π_{syn} values even larger than 0.5 indicating
127 that not only two, but multiple independent, non-syntenic haplotypes segregate implying that
128 these regions are more likely to undergo or conserve complex mutations as compared to the
129 rest of the genomes. Overall, we found 576 such hotspots of rearrangements (HR) with a total
130 size of 10.2 Mb including 351 regions in the gene-rich euchromatic chromosome arms with a
131 total length of 4.1 Mb (or 4% of euchromatic genome) (Supplementary Table 16).

132 Even though HRs in euchromatic regions included more transposable elements and less
133 genes as compared to conserved regions, they still contained significant numbers of genes,
134 many of which occurred at high and variable copy-number between the accessions (Fig. 3b,
135 c). For example, a HR on chromosome 4, which overlapped with the *RPP4/RPP5* R gene
136 cluster[24,25], displayed five to 15 intact or truncated copies of the *RPP5* gene within the eight
137 genomes (Fig. 3d and Supplementary Table 17). The different gene copies were primarily
138 introduced by an accumulation of forward tandem duplications and large indels (Fig. 3e), a
139 pattern, which was shared by many HR regions (Supplementary Fig. 5). While the individual
140 duplications were not conserved between the haplotypes, the borders of HRs were typically
141 well conserved (Fig. 3f). This suggested that either different selection regimes introduced
142 clear-cut borders between highly HRs and their surrounding regions, or that increased tandem
143 duplication rates were exactly limited to the HR regions. Such a local increase of mutation
144 rates could potentially be enabled by non-allelic homologous recombination (NAHR) which

145 could be triggered by the high number of local repeats in these regions[26–28]. In any case the
146 accession-specific accumulation of duplications suggested that the HR regions are only
147 partially linked to their genomic vicinity. To test this, we analysed the linkage disequilibrium
148 (LD) within 1,135 genomes of the 1001 Genomes Project[4] across the HR regions. LD was
149 high in the regions around the HR and was also high within HRs, however, when calculated
150 across the HR border LD was significantly lower supporting the idea that HRs are not linked
151 to the surrounding haplotypes but that they are segregating as large non-recombining units
152 (Fig. 4f). To test if HRs are indeed depleted for meiotic recombination, we overlapped them
153 with 15,683 crossover (CO) sites previously identified within Col-0/Ler F2 progenies[29,30]. Only
154 64 of them partially overlapped with non-syntenic regions while all other COs co-located
155 syntenic regions (Fig. 4b), suggesting that HRs are almost completely silenced for COs (P-
156 value < 2e-16) and that they follow different evolutionary dynamics as compared to the rest
157 of the (recombining) genome.

158 While lack of meiotic crossovers coupled with increased duplication rates can lead to
159 rapid generation of new haplotypes, reduced meiotic recombination also has been linked to
160 the accumulation of new (deleterious) mutations[31]. In agreement with this HRs also showed
161 an accumulation of single nucleotide polymorphisms with low allele frequencies and
162 potentially deleterious variation as compared to other regions in the genome (Fig. 4c, d and
163 Supplementary Fig. 6). Moreover, reduced recombination combined with geographic isolation
164 can provide the basis for the development of alleles, which are incompatible with distantly
165 related haplotypes leading to intra-species incompatibilities[32]. To test this, we searched the
166 location of nine recently reported genetic incompatible loci[33] (*DM1-9*) and found that all except
167 of one overlapped with HRs, while *DM3*, the locus which did not overlap with HRs, was closely
168 flanked by two HRs (Fig.5a and Supplementary Fig. 7-12). In addition, we also checked the
169 locus of a recently published single-locus genetic incompatibility[34] and found that it was also
170 residing in a HR region (Supplementary Fig. 13).

171 The excess of tandem duplications, accumulation of accession-specific gene-copy
172 numbers and increased sequence diversity paired with the lack of meiotic recombination and
173 the accumulation of deleterious alleles were reminiscent of the patterns that have been
174 described for R gene clusters[35–42]. In fact, the 808 reference genes in HRs were significantly
175 enriched for genes involved in defense response, signal transduction and secondary
176 metabolite biosynthesis (Fig. 4e) suggesting a reoccurring role of HRs in the adaptation to
177 biotic stress. As biotic challenges are constantly changing as pathogens evolve, it has been
178 proposed that the accumulation of new gene duplicates could increase the genomic diversity
179 and thereby enable rapid genomic changes supporting the genomic response of plants
180 against pathogens[28,43–45].

181 The availability of these high-quality, chromosome-level genomes assemblies now

182 enables the simultaneous access to all these regions, which can now be studied not only
183 locally, but in the context of entire genomes. For example, all but one of the 47 NB-LRR R-
184 gene clusters were completely reconstructed in all of the seven new assemblies (Fig. 5,
185 Supplementary Table 17)[46]. The completeness of the genomes allows an unbiased view on
186 all rearrangements, what could be essential as many of the HRs were only covered with a
187 few or even no allelic markers and could easily be missed with genome-wide selection or
188 diversity-scans (Supplementary Fig. 14 and 15). The genome-wide estimation of *Synteny*
189 *Diversity* might be one way to identify such regions which have the potential to act as the
190 genetic origin of rapid responses to the ever-changing environmental challenges.

191 Methods

192 Plant material and whole genome sequencing

193 The seeds of all seven accession were received from Maarten Koornneef (MPI for Plant
194 Breeding Research), and were grown under normal greenhouse conditions. DNA preparation
195 and next generation sequencing was performed by the Max Planck Genome center. The DNA
196 samples were prepared as previously described for the L*er*[9], and sequenced with a PacBio
197 Sequel system. For each accession, data from two SMRT cells were generated. Besides,
198 Illumina paired-end libraries were prepared and sequenced on the Illumina HiSeq2500
199 systems.

200 Genome assembly

201 PacBio reads were filtered for short (<50bp) or low quality (QV<80) reads using
202 SMRTLink5 package. *De novo* assembly of each genome was initially performed using three
203 different assembly tools including Falcon[47], Canu[48] and MECAT[49]. The resulting assemblies
204 were polished with Arrow from the SMRTLink5 package and then further corrected with
205 mapping of Illumina short reads using BWA[50] to remove small-scale assembly errors which
206 were identified with SAMTools[51]. For each genome, the final assembly was based on the
207 Falcon assembly as these assemblies always showed highest assembly contiguity. A few
208 contigs were further connected or extended based on whole genome alignments between
209 Falcon and Canu or MECAT assemblies. Contigs were labelled as organellar contigs if they
210 showed alignment identity and coverage both larger than 95% when aligned against the
211 mitochondrial or chloroplast reference sequences. A few of contigs aligned to multiple
212 chromosomes and were split if no Illumina short read alignments supported the conflicting
213 regions. Assembly contigs larger than 20kb were combined to pseudo-chromosomes
214 according to their alignment positions when aligned against the reference sequence using
215 MUMmer4[52]. Contigs with consecutive alignments were concatenated with a stretch of 500

216 Ns. To note, the assembly of the L*er* accession was already described in a recent study[9].

217 **Assembly evaluation**

218 We evaluated the assembly completeness by aligning the reference genes against each
219 of the seven genomes using Blastn[53]. Reference genes which were not aligned or only
220 partially aligned might reveal genes which were missed during the assembly. To examine
221 whether they were really missed, we mapped Illumina short reads from each genome against
222 the reference genome using the BWA[50] and checked the mapping coverage of these genes.
223 The genes, which were missing in the assembly, should show fully alignment coverage
224 (Supplementary Table 7).

225 Centromeric and telomeric tandem repeats were annotated by searching for the 178 bp
226 tandem repeat unit[54] and the 7 bp tandem repeat unit of TTTAGGG[55]. rDNA clusters were
227 annotated with Infernal version 1.1[56].

228 The assembly contiguity of Cvi-0 and L*er* were further tested using three previously
229 published genetic maps[57–59] (Supplementary Table 3). For this we aligned the marker
230 sequences against the chromosome-level assemblies and checked the order of the markers
231 in the assembly versus their order in the genetic map. The ordering of contigs to
232 chromosomes was perfectly supported by all three maps. Overall, only six (out of 1,156)
233 markers showed conflicts between the genetic and physical map. In all six cases we found
234 evidence that the conflict was likely caused by structural differences between the parental
235 genomes.

236 **Gene annotation**

237 Protein-coding genes were annotated based on *ab initio* gene predications, protein
238 sequence alignments and RNA-seq data. Three *ab initio* gene predication tools were used
239 including Augustus[60], GlimmerHMM[61] and SNAP[62]. The reference protein sequences from the
240 Araport 11[16] annotation were aligned to each genome assembly using exonerate[63] with the
241 parameter setting "--percent 70 --minintron 10 --maxintron 60000". For five accessions (An-1,
242 C24, Cvi-0, Ler-0, and Sha) we downloaded a total of 155 RNA-seq data sets from the NCBI
243 SRA database (Supplementary Table 8). RNA-seq reads were mapped to the corresponding
244 genome using HISAT2[64] and then assembled into transcripts using StringTie[65] (both with
245 default parameters). All different evidences were integrated into consensus gene models
246 using Evidence Modeler[66].

247 The resulting gene models were further evaluated and updated using the Araport 11[16]
248 annotation. Firstly, for each of the seven genomes, the predicted gene and protein sequences
249 were aligned to the reference sequence, while all reference gene and protein sequences were
250 aligned to each of the other seven genomes using Blast[53]. Then, potentially mis-annotated

genes including mis-merged (two or more genes are annotated as a single gene), mis-split (one gene is annotated as two or more genes) and unannotated genes were identified based on the alignments using in-house python scripts. Mis-annotated or unannotated genes were corrected or added by incorporating the open reading frames generated by *ab initio* predications or protein sequence alignment using Scipio[67].

Noncoding genes were annotated by searching the Rfam database[68] using Infernal version 1.1[56]. Transposon elements were annotated with RepeatMasker (http://www.repeatmasker.org). Disease resistance genes were annotated using RGAugury[69]. NB-LRR R gene clusters were defined based on the annotation from a previous study[70].

Pan-genome analysis

Pan-genome analyses were performed at both sequence and gene level. To construct a pan-genome of sequences, we generated pair-wise whole genome sequence alignments of all possible pairs of the eight genomes using the nucmer in the software package MUMmer4[52]. A pan-genome was initiated by choosing one of the genomes, followed by iteratively adding the non-aligned sequence of one of the remaining genomes. Here, non-aligned sequences were required to be longer than 100bp without alignment with an identity of more than 90%. The core genome was defined as the sequence space shared by all sampled genomes. Like the pan-genome, the core-genome analysis was initiated with one genome. Then all other genomes were iteratively added, while excluding all those regions which were not aligned against each of the other genomes. The pan- and core-genome of genes was built in a similar way. The pan-genome of genes was constructed by selecting the whole protein coding gene set of one of the accessions followed by iteratively adding the genes of one of the remaining accessions. Likewise, the core-genome of genes was defined as the genes shared in all sampled genomes.

For each pan or core genomes analysis, all possible ($\sum_{n=1}^{8}\left(\frac{8!}{n!(8-n)}\right)$) combinations of integrating the eight genomes (or a subset of them) were evaluated. The exponential regression model $y = A\,e^{Bx} + C$ to was then used to model the pan-genome/core-genomes by fitting medians using the least square method implemented in the nls function of R.

Analysis of structural rearrangements and gene CNV

All assemblies were aligned to the reference sequence using nucmer from the MUMmer4[52] toolbox with parameter setting "-max -l 40 -g 90 -b 100 -c 200". The resulting alignments were further filtered for alignment length (>100) and identity (>90). Structural rearrangements and local variations were identified using SyRI[9]. The functional effects of sequence variation were annotated with snpEff[71]. The gene CNV were identified according to the gene family clustering using the tool OrthoFinder[21] based on all protein sequences from

286 the eight accessions.

287 **Synteny diversity, hotspots of rearrangements and diversity estimates**

288 *Synteny Diversity* was defined as the average fraction of non-syntenic sites found within
289 all pairwise genome comparisons within a given population. Here we denote *Synteny*
290 *Diversity* as

291 $$\pi_{syn} = \sum_{ij} x_i x_j \pi_{ij},$$

292 where x_i and x_j refer to the frequencies of sequence i and j and π_{ij} to the average
293 probability of a position in i to be non-syntenic. Note, π_{syn} can be calculated in a given region
294 or for the entire genome. However even when calculated for small regions the annotation of
295 synteny still needs to established within the context of the whole genomes to avoid false
296 assignments of homologous but non-allelic sequence. Here we used the annotation of *SyRI*
297 to define syntenic regions. π_{syn} values can range from 0 to 1, with higher values referring to a
298 higher average degree of non-syntenic regions between the genomes.

299 For the analyses, we calculated π_{syn} in 5-kb sliding windows with 1kb step-size across the
300 entire genome. HR regions were defined as regions with π_{syn} larger than 0.5. Neighboring
301 regions were merged into one HR if their distance was shorter than 2kb.

302 The nucleotide and haplotype diversity were calculated with the R package PopGenome[72]
303 using SNP markers (with MAF > 0.05) from 1001 Genomes Project[4]. LD were calculated as
304 correlation coefficients r^2 using SNP markers with MAF > 0.05. GO enrichment analysis was
305 performed using the webtool DAVID[73,74].

Data availability

All raw sequencing data, assemblies and annotations can be accessed in the European Nucleotide Archive under the project accession number PRJEB31147.

Code availability

Custom code used in this study can be found online at *https://github.com/schneebergerlab/AMPRIL-genomes*.

Acknowledgements

The authors would like to thank Beth R. Rowan (UC Davis) for providing the CO breakpoint list, Bruno Hüttel (Max Planck Genome center) for support in genome sequencing, Sigi Effgen and Maarten Koornneef (Max Planck Institute for Plant Breeding Research) for providing seeds, Onur Dogan (Max Planck Institute for Plant Breeding Research) for help in the greenhouse, Angela M. Hancock (Max Planck Institute for Plant Breeding Research) for helpful discussions, and Raphael Mercier and Padraic J. Flood (Max Planck Institute for Plant Breeding Research) for helpful comments on the manuscript and the interpretation of HR regions.

Authors contributions

W.-B.J. and K.S. designed the study. W.-B.J. performed all analysis. K.S. supervised the study. W.-B.J. and K.S. wrote the manuscript. All authors read and approved the final manuscript.

Competing interests

The authors declare no competing interests.

327 # References

328

329 1. The Arabidopsis Genome Initiative. Analysis of the genome sequence of the flowering
330 plant Arabidopsis thaliana. *Nature* **408**, 796–815 (2000).
331 2. Cao, J. *et al.* Whole-genome sequencing of multiple Arabidopsis thaliana populations.
332 *Nat. Genet.* **43**, 956–965 (2011).
333 3. Long, Q. *et al.* Massive genomic variation and strong selection in Arabidopsis thaliana
334 lines from Sweden. *Nat. Genet.* **45**, 884–890 (2013).
335 4. Alonso-Blanco, C. *et al.* 1,135 Genomes Reveal the Global Pattern of Polymorphism
336 in Arabidopsis thaliana. *Cell* **166**, 481–491 (2016).
337 5. Schneeberger, K. *et al.* Reference-guided assembly of four diverse Arabidopsis
338 thaliana genomes. *PNAS* **108**, 10249–10254 (2011).
339 6. Gan, X. *et al.* Multiple reference genomes and transcriptomes for Arabidopsis thaliana.
340 *Nature* **477**, 419–423 (2011).
341 7. Schneeberger, K. *et al.* Simultaneous alignment of short reads against multiple
342 genomes. *Genome Biol.* (2009). doi:10.1186/gb-2009-10-9-r98
343 8. Schmitz, R. J. *et al.* Patterns of population epigenomic diversity. *Nature* (2013).
344 doi:10.1038/nature11968
345 9. Goel, M., Sun, H., Jiao, W.-B. & Schneeberger, K. SyRI: identification of syntenic and
346 rearranged regions from whole-genome assemblies. *bioRxiv* (2019).
347 doi:10.1101/546622
348 10. Zapata, L. *et al.* Chromosome-level assembly of Arabidopsis thaliana Ler reveals the
349 extent of translocation and inversion polymorphisms. *Proc. Natl. Acad. Sci.* **113**,
350 E4052–E4060 (2016).
351 11. Michael, T. P. *et al.* High contiguity Arabidopsis thaliana genome assembly with a
352 single nanopore flow cell. *Nat. Commun.* **9**, 1–8 (2018).
353 12. Pucker, B. *et al.* A chromosome-level sequence assembly reveals the structure of the
354 Arabidopsis thaliana Nd-1 genome and its gene set. *PLoS One* (2019).
355 doi:10.1371/journal.pone.0216233
356 13. Chin, C.-S. *et al.* Phased diploid genome assembly with single-molecule real-time
357 sequencing. *Nat Meth* **advance on**, (2016).
358 14. Huang, X. *et al.* Analysis of natural allelic variation in *Arabidopsis* using a multiparent
359 recombinant inbred line population. *Proc. Natl. Acad. Sci. U. S. A.* **108**, 4488–4493
360 (2011).
361 15. Jiao, W.-B. *et al.* Improving and correcting the contiguity of long-read genome
362 assemblies of three plant species using optical mapping and chromosome

363 conformation capture data. *Genome Res.* **27**, 778–786 (2017).
364 16. Cheng, C. Y. *et al.* Araport11: a complete reannotation of the Arabidopsis thaliana
365 reference genome. *Plant J.* (2017). doi:10.1111/tpj.13415
366 17. Loudet, O., Chaillou, S., Camilleri, C., Bouchez, D. & Daniel-Vedele, F. Bay-0 x
367 Shahdara recombinant inbred line population: A powerful tool for the genetic dissection
368 of complex traits in Arabidopsis. *Theor. Appl. Genet.* **104**, 1173–1184 (2002).
369 18. Simon, M. *et al.* Quantitative trait loci mapping in five new large recombinant inbred
370 line populations of Arabidopsis thaliana genotyped with consensus single-nucleotide
371 polymorphism markers. *Genetics* **178**, 2253–2264 (2008).
372 19. Tettelin, H. *et al.* Genome analysis of multiple pathogenic isolates of Streptococcus
373 agalactiae: Implications for the microbial 'pan-genome'. *Proc. Natl. Acad. Sci.* **102**,
374 13950–13955 (2005).
375 20. Medini, D., Donati, C., Tettelin, H., Masignani, V. & Rappuoli, R. The microbial pan-
376 genome. *Current Opinion in Genetics and Development* (2005).
377 doi:10.1016/j.gde.2005.09.006
378 21. Emms, D. M. & Kelly, S. OrthoFinder: solving fundamental biases in whole genome
379 comparisons dramatically improves orthogroup inference accuracy. *Genome Biol.*
380 (2015). doi:10.1186/s13059-015-0721-2
381 22. Durvasula, A. *et al.* African genomes illuminate the early history and transition to selfing
382 in *Arabidopsis thaliana*. *Proc. Natl. Acad. Sci.* **114**, 5213–5218 (2017).
383 23. Nei, M. & Li, W. H. Mathematical model for studying genetic variation in terms of
384 restriction endonucleases. *Proc. Natl. Acad. Sci.* (1979). doi:10.1073/pnas.76.10.5269
385 24. Parker, J. E. The Arabidopsis Downy Mildew Resistance Gene RPP5 Shares Similarity
386 to the Toll and Interleukin-1 Receptors with N and L6. *PLANT CELL ONLINE* (1997).
387 doi:10.1105/tpc.9.6.879
388 25. Van Der Biezen, E. A., Freddie, C. T., Kahn, K., Parker, J. E. & Jones, J. D. G.
389 Arabidopsis RPP4 is a member of the RPP5 multigene family of TIR-NB-LRR genes
390 and confers downy mildew resistance through multiple signalling components. *Plant J.*
391 **29**, 439–451 (2002).
392 26. Wicker, T., Yahiaoui, N. & Keller, B. Illegitimate recombination is a major evolutionary
393 mechanism for initiating size variation in plant resistance genes. *Plant J.* (2007).
394 doi:10.1111/j.1365-313X.2007.03164.x
395 27. Nagy, E. D. & Bennetzen, J. L. Pathogen corruption and site-directed recombination at
396 a plant disease resistance gene cluster. *Genome Res.* (2008).
397 doi:10.1101/gr.078766.108
398 28. Leister, D. Tandem and segmental gene duplication and recombination in the evolution
399 of plant disease resistance genes. *Trends in Genetics* (2004).

400 doi:10.1016/j.tig.2004.01.007
401 29. Serra, H. *et al.* Massive crossover elevation via combination of HEI10 and recq4a
402 recq4b during Arabidopsis meiosis . *Proc. Natl. Acad. Sci.* (2018).
403 doi:10.1073/pnas.1713071115
404 30. Rowan, B. A. *et al.* An ultra high-density Arabidopsis thaliana crossover map that
405 refines the influences of structural variation and epigenetic features. *bioRxiv* (2019).
406 doi:10.1101/665083
407 31. Kondrashov, A. S. Deleterious mutations and the evolution of sexual reproduction.
408 *Nature* (1988). doi:10.1038/336435a0
409 32. Bomblies, K. & Weigel, D. Hybrid necrosis: Autoimmunity as a potential gene-flow
410 barrier in plant species. *Nat. Rev. Genet.* **8**, 382–393 (2007).
411 33. Chae, E. *et al.* Species-wide genetic incompatibility analysis identifies immune genes
412 as hot spots of deleterious epistasis. *Cell* **159**, 1341–1351 (2014).
413 34. Smith, L. M., Bomblies, K. & Weigel, D. Complex evolutionary events at a tandem
414 cluster of Arabidopsis thaliana genes resulting in a single-locus genetic incompatibility.
415 *PLoS Genet.* **7**, (2011).
416 35. Michelmore, R. W. & Meyers, B. C. Clusters of resistance genes in plants evolve by
417 divergent selection and a birth-and-death process. *Genome Research* (1998).
418 doi:10.1101/gr.8.11.1113
419 36. Meyers, B. C., Shen, K. A., Rohani, P., Gaut, B. S. & Michelmore, R. W. Receptor-like
420 genes in the major resistance locus of lettuce are subject to divergent selection. *Plant*
421 *Cell* (1998). doi:10.1105/tpc.10.11.1833
422 37. Noel, L. Pronounced Intraspecific Haplotype Divergence at the RPP5 Complex
423 Disease Resistance Locus of Arabidopsis. *Plant Cell Online* **11**, 2099–2112 (1999).
424 38. McDowell, J. M. *et al.* Intragenic recombination and diversifying selection contribute to
425 the evolution of downy mildew resistance at the RPP8 locus of arabidopsis. *Plant Cell*
426 (1998). doi:10.1105/tpc.10.11.1861
427 39. Botella, M. A. *et al.* Three genes of the arabidopsis RPP1 complex resistance locus
428 recognize distinct Peronospora parasitica avirulence determinants. *Plant Cell* (1998).
429 doi:10.1105/tpc.10.11.1847
430 40. Barragan, C. A. *et al.* RPW8/HR repeats control NLR activation in Arabidopsis thaliana.
431 *PLOS Genet.* (2019). doi:10.1371/journal.pgen.1008313
432 41. Bakker, E. G. A Genome-Wide Survey of R Gene Polymorphisms in Arabidopsis. *Plant*
433 *Cell Online* **18**, 1803–1818 (2006).
434 42. Guo, Y.-L. *et al.* Genome-Wide Comparison of Nucleotide-Binding Site-Leucine-Rich
435 Repeat-Encoding Genes in Arabidopsis. *Plant Physiol.* **157**, 757–769 (2011).
436 43. Dangl, J. L. & Jones, J. D. G. Plant pathogens and integrated defence responses to

437 infection. *Nature* (2001). doi:10.1038/35081161
438 44. Boller, T. & He, S. Y. Innate immunity in plants: An arms race between pattern
439 recognition receptors in plants and effectors in microbial pathogens. *Science* (2009).
440 doi:10.1126/science.1171647
441 45. Kondrashov, F. A. Gene duplication as a mechanism of genomic adaptation to a
442 changing environment. *Proceedings of the Royal Society B: Biological Sciences* (2012).
443 doi:10.1098/rspb.2012.1108
444 46. Choi, K. *et al.* Recombination Rate Heterogeneity within Arabidopsis Disease
445 Resistance Genes. *PLoS Genet.* (2016). doi:10.1371/journal.pgen.1006179
446 47. Chin, C.-S. *et al.* Phased diploid genome assembly with single-molecule real-time
447 sequencing. *Nat Methods* **13**, 1050–1054 (2016).
448 48. Koren, S. *et al.* Canu: scalable and accurate long-read assembly via adaptive k-mer
449 weighting and repeat separation. *Genome Res.* (2017). doi:10.1101/gr.215087.116
450 49. Xiao, C. Le *et al.* MECAT: Fast mapping, error correction, and de novo assembly for
451 single-molecule sequencing reads. *Nat. Methods* **14**, 1072–1074 (2017).
452 50. Li, H. & Durbin, R. Fast and accurate short read alignment with Burrows-Wheeler
453 transform. *Bioinformatics* **25**, 1754–1760 (2009).
454 51. Li, H. *et al.* The Sequence Alignment/Map format and SAMtools. *Bioinformatics* **25**,
455 2078–2079 (2009).
456 52. Marçais, G. *et al.* MUMmer4: A fast and versatile genome alignment system. *PLoS*
457 *Comput. Biol.* (2018). doi:10.1371/journal.pcbi.1005944
458 53. Altschul, S. F., Gish, W., Miller, W., Myers, E. W. & Lipman, D. J. Basic local alignment
459 search tool. *J. Mol. Biol.* (1990). doi:10.1016/S0022-2836(05)80360-2
460 54. Heslop-Harrison, J. S., Murata, M., Ogura, Y., Schwarzacher, T. & Motoyoshi, F.
461 Polymorphisms and Genomic Organization of Repetitive DNA from Centromeric
462 Regions of Arabidopsis Chromosomes. *Plant Cell* **11**, 31 LP – 42 (1999).
463 55. Richards, E. J. & Ausubel, F. M. Isolation of a higher eukaryotic telomere from
464 Arabidopsis thaliana. *Cell* (1988). doi:10.1016/0092-8674(88)90494-1
465 56. Nawrocki, E. P. & Eddy, S. R. Infernal 1.1: 100-fold faster RNA homology searches.
466 *Bioinformatics* (2013). doi:10.1093/bioinformatics/btt509
467 57. Simon, M. *et al.* Quantitative trait loci mapping in five new large recombinant inbred
468 line populations of *Arabidopsis thaliana* genotyped with consensus single-nucleotide
469 polymorphism markers. *Genetics* (2008). doi:10.1534/genetics.107.083899
470 58. Singer, T. *et al.* A high-resolution map of Arabidopsis recombinant inbred lines by
471 whole-genome exon array hybridization. *PLoS Genet.* (2006).
472 doi:10.1371/journal.pgen.0020144
473 59. Giraut, L. *et al.* Genome-wide crossover distribution in Arabidopsis thaliana meiosis

474 reveals sex-specific patterns along chromosomes. *PLoS Genet.* (2011).
475 doi:10.1371/journal.pgen.1002354
476 60. Stanke, M. & Waack, S. Gene prediction with a hidden Markov model and a new intron
477 submodel. *Bioinformatics* **19**, (2003).
478 61. Majoros, W. H., Pertea, M. & Salzberg, S. L. TigrScan and GlimmerHMM: Two open
479 source ab initio eukaryotic gene-finders. *Bioinformatics* (2004).
480 doi:10.1093/bioinformatics/bth315
481 62. Korf, I. Gene finding in novel genomes. *BMC Bioinformatics* (2004). doi:10.1186/1471-
482 2105-5-59
483 63. Slater, G. S. C. & Birney, E. Automated generation of heuristics for biological sequence
484 comparison. *BMC Bioinformatics* **6**, 31 (2005).
485 64. Kim, D., Langmead, B. & Salzberg, S. L. HISAT: A fast spliced aligner with low memory
486 requirements. *Nat. Methods* (2015). doi:10.1038/nmeth.3317
487 65. Pertea, M. *et al.* StringTie enables improved reconstruction of a transcriptome from
488 RNA-seq reads. *Nat. Biotechnol.* (2015). doi:10.1038/nbt.3122
489 66. Haas, B. J. *et al.* Automated eukaryotic gene structure annotation using
490 EVidenceModeler and the Program to Assemble Spliced Alignments. *Genome Biol.* **9**,
491 R7 (2008).
492 67. Keller, O., Odronitz, F., Stanke, M., Kollmar, M. & Waack, S. Scipio: Using protein
493 sequences to determine the precise exon/intron structures of genes and their orthologs
494 in closely related species. *BMC Bioinformatics* **9**, 1–12 (2008).
495 68. Kalvari, I. *et al.* Rfam 13.0: Shifting to a genome-centric resource for non-coding RNA
496 families. *Nucleic Acids Res.* (2018). doi:10.1093/nar/gkx1038
497 69. Li, P. *et al.* RGAugury: A pipeline for genome-wide prediction of resistance gene
498 analogs (RGAs) in plants. *BMC Genomics* (2016). doi:10.1186/s12864-016-3197-x
499 70. Choi, K. *et al.* Recombination Rate Heterogeneity within Arabidopsis Disease
500 Resistance Genes. *PLoS Genet.* **12**, 1–30 (2016).
501 71. Cingolani, P. *et al.* A program for annotating and predicting the effects of single
502 nucleotide polymorphisms, SnpEff: SNPs in the genome of Drosophila melanogaster
503 strain w1118; iso-2; iso-3. *Fly (Austin).* (2012). doi:10.4161/fly.19695
504 72. Pfeifer, B., Wittelsbürger, U., Ramos-Onsins, S. E. & Lercher, M. J. PopGenome: An
505 efficient swiss army knife for population genomic analyses in R. *Mol. Biol. Evol.* **31**,
506 1929–1936 (2014).
507 73. Huang, D. W., Sherman, B. T. & Lempicki, R. A. Systematic and integrative analysis of
508 large gene lists using DAVID bioinformatics resources. *Nat. Protoc.* (2009).
509 doi:10.1038/nprot.2008.211
510 74. Huang, D. W., Sherman, B. T. & Lempicki, R. A. Bioinformatics enrichment tools: Paths

511 toward the comprehensive functional analysis of large gene lists. *Nucleic Acids Res.*
512 (2009). doi:10.1093/nar/gkn923
513
514

515 # Tables

516 **Table 1. Genome assembly and annotation of eight *A. thaliana* accessions**

	Col-0	An-1	C24	Cvi-0	Eri-1	Kyo	L*er*	Sha
Total sequences	5	151	167	140	200	230	149	143
Total length (Mbp)	119.1	120.1	119.2	119.7	120.8	122.2	120.3	120.3
Contig N50 (Mbp)	-	8.2	4.8	7.4	4.8	9.1	11.2	7.0
Contig L50	-	6	8	7	8	6	5	6
Contig N90 (Mbp)	-	1.3	0.6	2.0	0.7	0.9	0.8	1.0
Contig L90	-	17	34	17	34	19	18	23
CL50	-	2	2	2	2	2	1	1
Chr. Length (Mbp)	119.1	118.4	117.7	118.3	117.7	118.8	118.5	118.4
Genes	27,445	27,342	27,214	27,098	27,285	27,574	27,376	27,293

517

518 # Figure legends

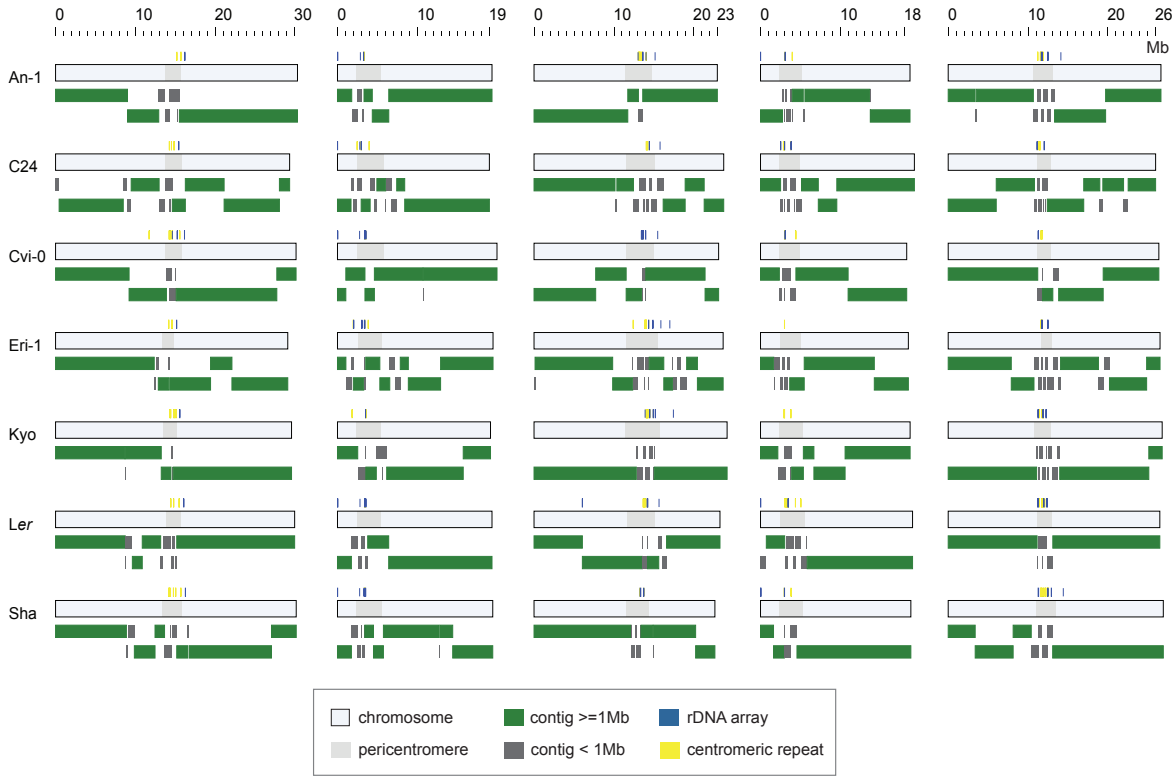

519

520

521 **Figure 1. Chromosome-level genome assemblies of seven *A. thaliana* accessions.**
522 The arrangement of contigs to chromosomes for seven assemblies are shown with green (>1
523 Mb) and dark grey (<1 Mb) boxes. The full range of each chromosomes is shown with a light
524 blue bar, where the gray inlays outline the extend of the pericentromeric regions. The location
525 of centromeric tandem repeat arrays and rDNA clusters within the assemblies are marked by
526 yellow and blue bars above each of the chromosomes.

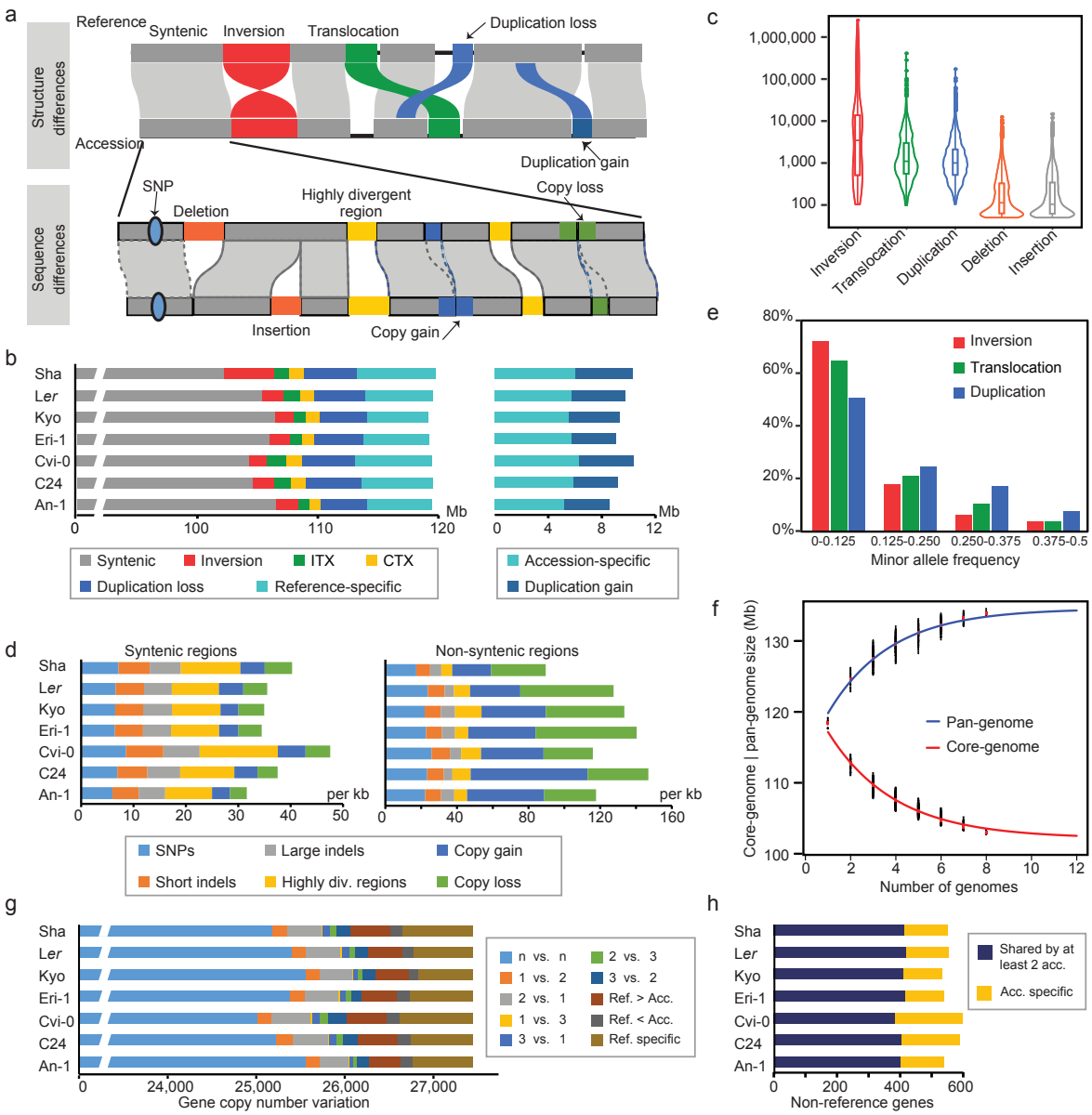

Figure 2. Comprehensive catalogue of structural variation

(a) Schematic of the structural differences (upper panel) and local sequence variation (lower panel) that can be identified by whole-genome comparisons using SyRI[9]. Note, local sequence variation can reside in syntenic as well as in rearranged regions. **(b)** The total span of syntenic and rearranged regions between the reference and each of other accessions. The left plot shows the sequence span in respect to the reference sequence, while the right plot shows the sequence space, which is specific to each of the accessions. **(c)** Size distributions of different types of structural variation. **(d)** Local variation (per kb) in syntenic (left) and rearranged (right) regions between the reference and each of other accessions. **(e)** Minor allele frequencies of all three types of rearranged regions. **(f)** Pan-genome and core-genome estimations based on all pairwise whole-genome comparisons across all eight accessions. Each point corresponds to a pan- or core-genome size estimated with a particular

541 combination of genomes. The red points indicate median values for each combination with
542 the same number of genomes. Pan-genome (blue) and core-genome (red) estimations were
543 fitted using an exponential model. **(g)** Gene copy number variations (CNV) between the
544 reference and each of the accessions group by differences in the gene families: n *vs*. n: both
545 the reference and the query genomes have the same number of genes in a gene family.
546 Others categories (1 *vs*. 2, 2 *vs*. 1, 1 *vs*. 3, 3 *vs*. 1, 2 *vs*. 3 and 3 *vs* 2) indicate the number of
547 reference and accession genes in the gene families with the respective size differences. “Ref. >
548 Acc.” and “Ref. < Acc.” refer to all remaining gene families where either the reference or the
549 accession has more genes. “Ref. specific” refers to gene families which are only present in
550 the reference genome. **(h)** The number of non-reference genes found in at least two
551 accessions (blue), or found to be specific to an accession genome (yellow).

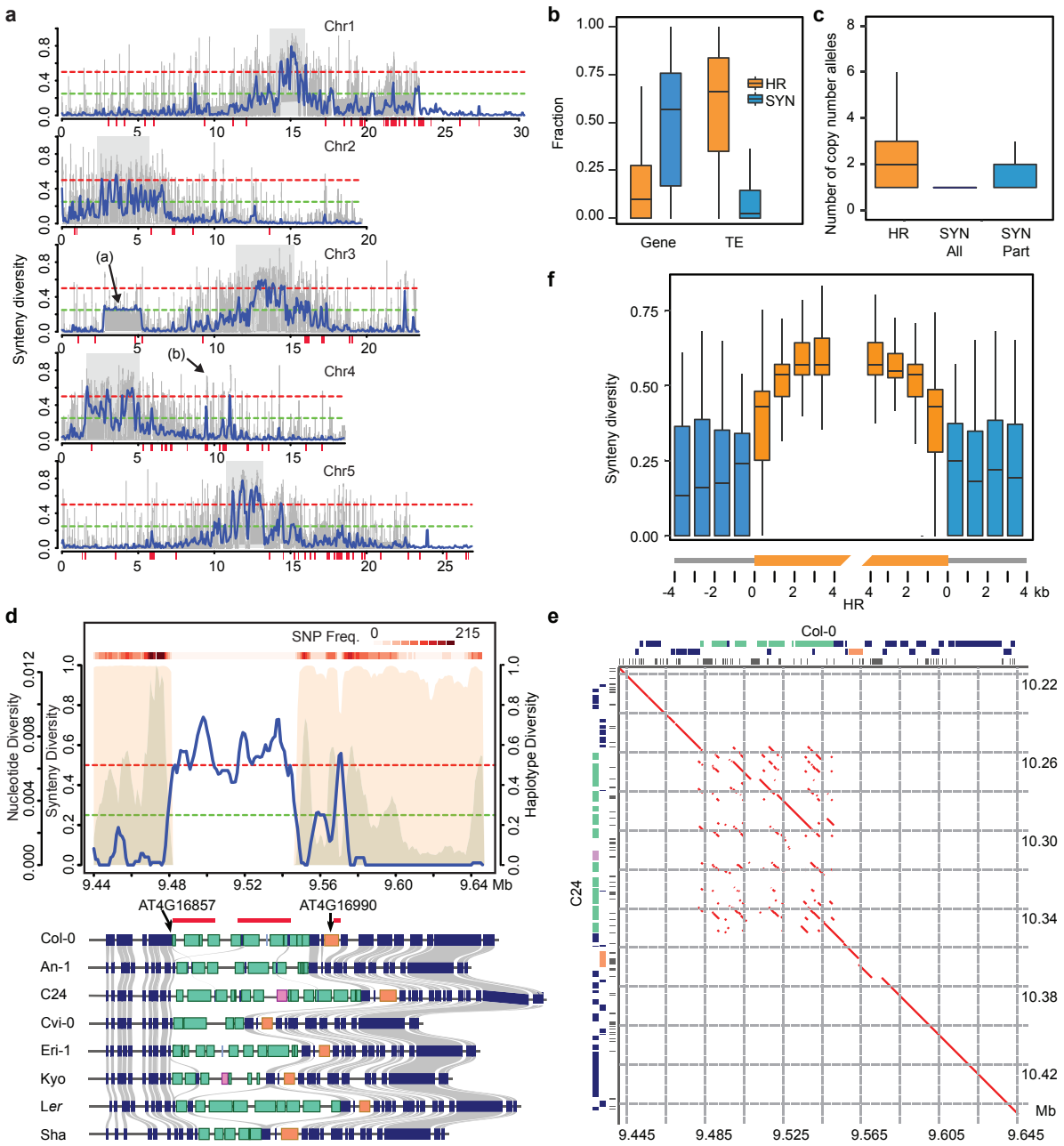

Figure 3. Hotspots of rearrangements revealed by *Synteny Diversity*

(a) Synteny Diversity calculated along each chromosome; in blue: 100kb sliding windows with a step-size of 50kb; in grey: 5kb sliding windows with a step-size of 1kb. The red bars under the x-axes indicate the location of R gene clusters. Gray rectangles indicate the location of centromeric regions. The dashed green and red lines indicate thresholds for Synteny Diversity values of 0.25 and 0.50 indicative for the segregation of two (0.25) or three (0.50) non-syntenic haplotypes (in a population of eight genomes). The arrow labelled with "(a)" indicates a region of a 2.48 Mb inversion in the Sha genome. The arrow labelled with "(b)" indicates the location of the example region show in (d). **(b)** Gene and TE densities in syntenic (SYN) and hotspots of rearrangements (HR) regions. **(c)** Distribution of different copy-number alleles in

564 syntenic regions (SYN-All), hotspots of rearrangements (HR) and the remaining, partially
565 syntenic regions (SYN-Part)**. (d)** An example of an HR region which includes the *RPP4/RPP5*
566 R gene cluster. The upper panel shows the distribution of Synteny Diversity (blue curve),
567 nucleotide diversity (gray background) and haplotype diversity (pink background) in a 5kb
568 sliding window with a step-size of 1kb. Both the nucleotide diversity and the haplotype
569 diversity were calculated based on the informative markers (MAF >= 0.05, missing rate < 0.2)
570 from the 1001 Genomes Project[4]. The green and red dashed lines indicate the value 0.25 and
571 0.50 of synteny diversity, respectively. The marker density is shown as the heatmap on top.
572 The schematic in the lower part shows the location of the protein-coding genes (rectangles)
573 annotated in each of the eight genomes. In blue, gene without function implicated in disease
574 resistance. Other colored rectangles represent the resistance genes, where genes with the
575 same color belong to the same gene family. The gray links between the rectangles indicate
576 the homolog relationship of non-resistance genes. The red lines indicate the positions of HRs**.**
577 **(e)** A dot plot of Col-0 and C24 from the HR region shown in (d), where the red lines show the
578 regions with substantial homology between the two genomes. The three rows on top and the
579 three columns on the right show the location of genes on the forward strand (top), on the
580 reverse strand (middle) and the repeat regions (bottom). Genes are colored as in (d). **(f)** The
581 distribution of Synteny Diversity values in 1kb sliding windows around and in all HRs.
582

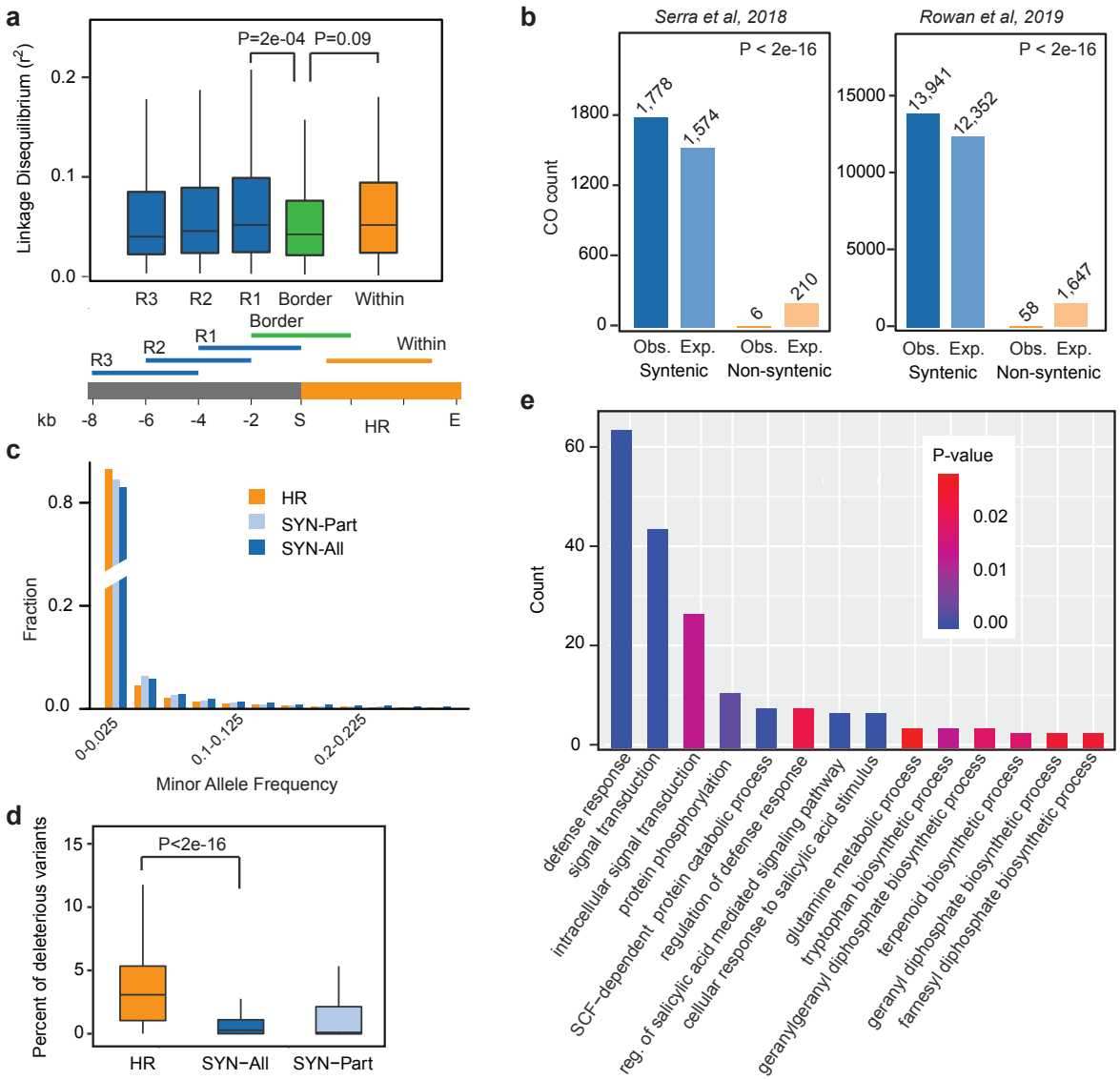

Figure 4. Evolutionary implications of hotspot of rearranged regions

(a) Linkage disequilibrium (LD) calculated in 4kb windows in and around each of the HRs. R1, R2 and R3 refer to 4kb windows up-/down-stream of each HR; "Within" refers to the 4kb in the center of the HRs; "Border" refers to the 4kb windows centered on each of the two borders of each HR. LD was calculated as the correlation coefficient (r^2) based on informative SNP markers (MAF > 0.05, missing rate < 0.2) from 1001 Genomes Project[4]. **(b)** Recently assessed crossover (CO) breakpoint sites[29,30] in syntenic and non-syntenic regions. Only unique CO intervals smaller than 5kb were used. Chi-square test was applied. **(c)** Fraction of SNP markers from SYN-All, SYN-Part and HRs regions across different minor allele frequency bins. The SNP markers (MAF >0.005, missing rate < 0.2) from 1001 Genomes Project were used. **(d)** Frequency of deleterious mutations in syntenic regions (SYN-All), hotspots of rearrangements (HR) and the remaining, partially syntenic regions (SYN-Part). Deleterious mutations include SNPs and small indels that introduce premature stop codons,

598 loss of start or stop codons, frameshifts, splicing sites mutations or deletions of exons. (e) GO
599 term enrichment analysis of protein-coding genes in HR regions (P-values cut-off = 0.05).
600

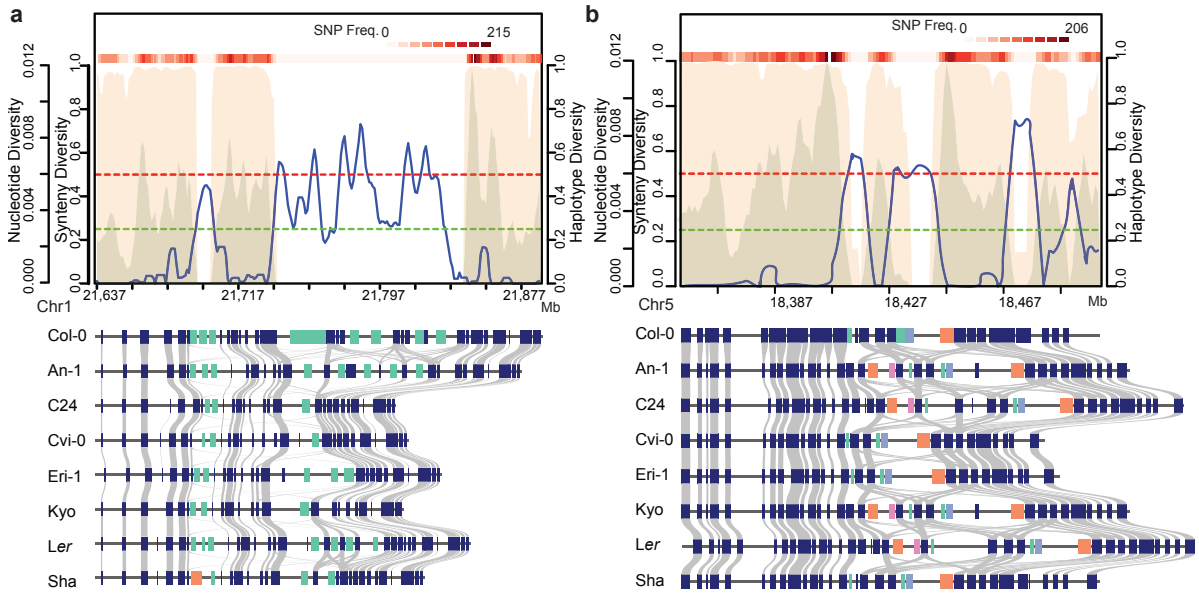

Figure 5. Two examples for R gene clusters identified as hotspots of rearrangements. Visualization of **(a)** the *DM6* locus (*RPP7*)[33] and **(b)** an unnamed R gene cluster on chromosome 5. Descriptions for the plots can be found in the legend of Fig. 3d.